Material and technology developments of the totally sputtering-made *p/n* GaN diodes for cost-effective power electronics

Cheng-Che Li · Dong-Hau Kuo

Abstract Mg-doped GaN (Mg–GaN) films have been deposited on Si (100) substrates by radio-frequency reactive sputtering technique with single cermet targets. The targets can be made by hot pressing the mixture of metallic Ga and Mg powders and ceramic GaN powder. X-ray diffraction results showed that Mg–GaN films had a wurtzite structure with a preferential nonpolar $m - (10\bar{1}0)$ growth plane. Mg–GaN with 10.2 % Mg has transformed into *p*-type conductivity and has the carrier concentration of 9.37×10^{16} cm^{-3}, the highest mobility of 345 cm^2 V^{-1} s^{-1}, and the highest conductivity of 3.23 S cm^{-1}. The band gap of Mg–GaN films retrieved from the absorption spectra is 2.93–3.06 eV. Furthermore, we have also fabricated a totally sputtering-made and cost-effective GaN diode with the ideality factors of 5.0 and 4.9 for the as-deposited and the annealed, respectively.

1 Introduction

In the past two decades, GaN and its alloys successfully applied to light emission devices, such as light emitting diodes (LEDs) and laser diodes (LD) [1–3]. GaN is an important semiconductor material due to its direct band gap of 3.4 eV and other excellent characteristics such as high breakdown voltage, high mobility, and thermal stability [4]. There are several approaches for depositing GaN films, such as metal organic chemical vapor deposition (MOC-VD) [1, 5] and molecular beam epitaxy (MBE) [6].

C.-C. Li · D.-H. Kuo (✉)
Department of Materials Science and Engineering, National Taiwan University of Science and Technology, Taipei 10607, Taiwan
e-mail: dhkuo@mail.ntust.edu.tw

In the early 1990s, S. Nakamura group demonstrated an important work in growing Mg–GaN films at 1,000 °C by MOCVD, where trimethylgallium (TMG), ammonia (NH$_3$), and bis-cyclopentadienyl magnesium (Cp$_2$Mg) were used as Ga, N, and Mg sources, respectively. They improved the film resistivity by thermal annealing process. After 700 °C thermal annealing in nitrogen atmosphere, the Mg–GaN films exhibited *p*-type conductivity. Their hole concentration and mobility were 3.0×10^{17} cm^{-3} and 10 cm^2 V^{-1} s^{-1}, respectively [7]. In the recent research, Ke et al. [8] indicated that smooth *p*-type GaN films should be deposited under a very low pressure of 50 mbar by MOCVD. Their hole concentration was changed from 4.7×10^{16} cm^{-3} to 3.1×10^{17} cm^{-3} with increasing the Cp$_2$Mg flow rate. In addition, there are several other methods to increase the hole concentration of *p*-type GaN films, such as delta-doping method [9], Mg–O doping [10], and multilayered buffer [11]. However, high fabrication cost and process temperature are the major challenges for MOCVD process. On the contrary, the GaN films have also been deposited on Si substrate by sputtering. If the Ga target is adopted, it becomes a viscous state due to the melting temperature (T$_m$) of 29 °C. If the GaN target is used, its fabrication is difficult due to T$_m$ > 2,500 °C. Zhang et al. [12] deposited GaN films at 500 °C by sputtering with Ga target in pure nitrogen atmosphere. Kim et al. [13] deposited GaN films by sputtering with a GaN target in pure Ar atmosphere. Furthermore, polarization-induced doping in nitrides received a lot of attention. Li et al. and Simon et al. [14–16] had investigated the Al$_x$Ga$_{1-x}$N layer grown by MBE. However, there is no report on the growth of *p*-type GaN films by sputtering.

In this research, we attempt to deposit *p*-type GaN films by rf reactive sputtering with single Mg-containing cermet targets. The cermet targets were made by mixture metallic

Mg and Ga and ceramic GaN powder, by which the viscous problem of the Ga target during sputtering can be overcome. Sputtering technique is a cost-effective, environmentally safe, and mass production process. *p*-type GaN, an important component for devices, made by reactive sputtering instead of MOCVD and MBE is still intriguing. Thermally stable GaN electronic devices such as *p/n* and Schottky diodes can have potential applications for power electronics. The formation of *p*-type Mg–GaN is being explored and demonstrated without the need of thermal annealing. To further identify the *p*-type behavior, a *p/n* GaN diode device totally made by sputtering has been fabricated and evaluated.

2 Experimental details

Mg–GaN films were grown on Si (100) substrates by rf reactive sputtering technique with single cermet targets. The cermet targets were prepared by hot pressing the mixture of metallic Ga and Mg powders and ceramic GaN powder at 300–500 °C for 30 min in inert atmosphere. The Mg contents in the four kinds of cermet targets were 0, 5, 10, and 15 at.%. Their corresponding films were symbolized as Mg-*x* GaN with *x* = 0, 0.05, 0.1, and 0.15. The Ga/(Ga + GaN) molar ratio in each cermet target was kept at 0.3. To get rid of the oxygen contamination, the sputter chamber was pumped to a pressure less than 1×10^{-6} torr before sputtering. The deposition temperature and sputtering power were kept at 400 °C and 150 W, respectively. The deposition time was 60 min. The plasma working pressure was kept at 9×10^{-3} torr. The sputtering process was under the gas mixture of Ar and N_2 with a flow rate of 5 sccm for each. Furthermore, we also designed a *p/n* GaN diode for measuring its electrical property. The *p/n* GaN diode with a homojunction was deposited on Pt/TiO$_2$/Si substrate. The *n*- and *p*-type GaN films for diode were made of Mg-0 GaN and Mg-0.1 GaN, respectively. The sizes of each Al electrodes were 1 mm^2.

The structure of Mg-*x* GaN films was identified by X-ray diffraction (XRD, D8 Discover, Bruker). Scanning electron microscope (SEM, JSM-6500F, JEOL) was used to observe the surface morphology and cross-sectional image of Mg–GaN films. Energy dispersive spectrometer (EDS, JSM-6500F, JEOL) equipped on SEM was used for composition analysis. Surface root-mean-square (rms) roughness of Mg–GaN films was evaluated by atomic force microscopy (AFM, Dimension Icon, Bruker). Three measurements were conducted on each specimen. Carrier concentration, mobility, and electrical conductivity of Mg–GaN films were measured by Hall measurement (HMS-2000, Ecopia) with a maximum magnetic field of 0.51 T. The samples for Hall measurement had four
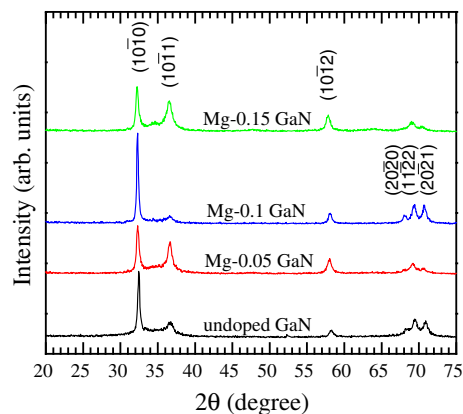

Fig. 1 XRD diffraction patterns of Mg–GaN films deposited at 400 °C with different magnesium contents in targets

electrical contacts made of silver paste, which was dried in an oven at 100 °C for 10 min. Ultraviolet–visible (UV–vis) spectrometer (V-670, Jasco) was used to measure the absorption spectra for Mg–GaN films deposited on glass substrates. The rectifying behavior of a *p/n* GaN diode with a homojunction was measured by semiconductor device analyzer (B1500A, Agilent).

3 Results and discussion

Figure 1 shows the X-ray diffraction patterns of Mg–GaN films grown on Si (100) substrates with different Mg contents. Mg–GaN films showed a wurtzite structure and had preferentially grown with the nonpolar *m*-(10$\bar{1}$0) crystal plane. Considering the minimization of surface energy to lower the total free energy, the sputtered GaN film prefers to grow with a (10$\bar{1}$0) crystal plane of low surface energy of 118 meV/Å^2 instead of 125 meV/Å^2 for the (0001) plane [17]. The same diffraction results were also occurred, as the (0001) sapphire substrate was used for deposition. With our deposition condition, the thermodynamically stable growth plane is not the (0001) plane and the epitaxial growth of GaN on the (0001) sapphire substrate needs to be further investigated. No second phases had been detected, which indicated the Mg incorporation into GaN to form a solid solution or the Mg cation substituted the lattice site of the Ga cation. The nonpolar *m*-(10$\bar{1}$0) peak position of the undoped GaN film located at $2\theta = 32.49°$ and the peak position was slightly shifted to lower 2θ values of 32.32°, 32.28°, and 32.24° as the Mg-doping content in targets increased from 5, 10, to 15 at.%, respectively. Table 1 lists the lattice constants (*a* and *c*), unit cell volume, and full-width at half-maximum (FWHM) of the (10$\bar{1}$0) diffraction peak of the Mg-*x* GaN films. The values of *a, c* and unit cell volume were increased with

Table 1 Lattice constants, unit cell volume, and full-width at half-maximum (FWHM) of Mg-x GaN films at $x = 0$, 0.05, 0.1, and 0.15

Cermet target	2θ (10$\bar{1}$0) peak	a (Å)	c (Å)	volume (Å^3)	FWHM (10$\bar{1}$0) (2θ°)
GaN	32.49	3.183	5.198	45.61	0.30
Mg-0.05 GaN	32.32	3.198	5.222	46.25	0.34
Mg-0.1 GaN	32.28	3.201	5.227	46.38	0.25
Mg-0.15 GaN	32.24	3.207	5.237	46.64	0.30

Table 2 Compositional analyses of Mg-doped GaN films deposited with different Mg contents in targets

Cermet target	Ga (at.%)	Mg (at.%)	N (at.%)	Mg/ (Mg + Ga)	N/ (Mg + Ga)
GaN	54.98	–	45.02	–	0.819
Mg-0.05 GaN	51.97	3.13	44.90	0.056	0.815
Mg-0.1 GaN	49.14	5.64	45.22	0.102	0.825
Mg-0.15 GaN	48.37	6.31	45.32	0.115	0.829

increasing the Mg content. Basically, the substitution of the smaller Ga^{3+} ion [r(Ga^{3+}) = 0.62 Å of effective ionic radius] [18] in GaN with the larger Mg^{2+} ion [r(Mg^{2+}) = 0.72Å] leads to the lattice expansion, the shift of diffraction peak to a smaller 2θ value, and slightly larger lattice parameters.

The compositional analyses for Mg–GaN films are shown in Table 2. With the EDS analysis results, the N/(Ga + Mg) ratio were 0.819, 0.815, 0.825 and 0.829 for Mg-x GaN films at $x = 0$, 0.05, 0.1, and 0.15, respectively. The nitrogen deficiency in all Mg-x GaN films with a close N/(Ga + Mg) ratio was in a close degree and its influence on lattice parameters should be similar and was not an affecting factor. For the Mg/(Mg + Ga) ratio, it was 5.6, 10.2, and 11.5 % for Mg-x GaN at $x = 0.05$, 0.1, and 0.15, respectively. These data indicate that up to 10 %Mg in target can produce Mg–GaN with ∼10 % Mg in film. With a high Mg content of 15 % in target, the Mg content in Mg–GaN films has only increased to 11.5 %. Therefore, the solubility of Mg into the Ga lattice of GaN can be close to 10 %.

Figure 2 shows SEM surface images of Mg–GaN films deposited at 400 °C by sputtering. During the 400 °C deposition, Mg–GaN films were smooth and crack- and pore-free. The average grain sizes of Mg–GaN films were around 26 ± 1 nm. The cross-sectional images were individually shown in the insets. The undoped GaN film showed a columnar structure. As the Mg-doping content increased to 5.6 at.%, the column structure of Mg-0.05 GaN in Fig. 2b was not as clear as that of undoped one. The column structure disappeared and there were no apparent features as the Mg content in Mg-0.1 GaN reached 10.2 at.%. From the

cross-sectional images, the thickness values of Mg–GaN were measured to be 2.12, 2.11, 2.12, and 2.33 μm for Mg-x GaN at $x = 0$, 0.05, 0.1, and 0.15, respectively. The corresponding growth rates were calculated to be 35.3, 35.1, 35.4, and 38.9 nm/min. The addition of Mg dopant into GaN obviously has no effects on growth rate. Although the reported deposition rates for GaN films by MOCVD and MBE were 8.3–25 nm/min, their films had an epitaxial growth [19, 20]. Our rf sputtering technique provided a faster approach for depositing polycrystalline Mg–GaN films. Although there is a big difference in the thermal expansion coefficients of GaN (5.59×10^{-6} K^{-1}) and Si (3.59×10^{-6} K^{-1}) [21], the 2 μm-thick Mg–GaN films do not show any interfacial cracking or delamination between Mg and GaN films and Si substrate after deposition at 400 °C, which can be attributed to the polycrystalline nature of the preferentially grown GaN films. The fact of the Mg-0.1 and Mg-0.15 GaN films with the featureless microstructure is related to the change in nucleation behavior. The Mg doping disturbs the reactions between Ga and N adatoms to form GaN nuclei, therefore the smaller nuclei formed at a higher Mg content lead to a featureless growth mode. Due to the smaller nuclei, more defects such as grain boundary, stacking fault, dislocation et al. are also expected.

Figure 3 shows AFM morphologies of Mg–GaN films at different Mg contents. The root-mean-square (rms) roughness of undoped GaN film was 3.23 ± 0.04 nm. With the increase in the Mg-doping content, the rms roughness of Mg-x GaN at $x = 0.05$, 0.1, and 0.15 slightly increased from 3.33 ± 0.03, 3.74 ± 0.12, to 4.10 ± 0.04 nm, respectively. The similar phenomena had been report for Mg–GaN films deposited by MOCVD. Ke et al. [8] observed the rms roughness of Mg–GaN films was 0.72–23.45 nm with the rougher film at the higher Mg content. The surface roughness of Mg–GaN has been attributed to a difference in atomic size between Ga and Mg, which made the lattice distortion, dislocation generation, and growth in three dimensions [22]. The rougher surface for our Mg–GaN films can be attributed to the lower deposition temperature at 400 °C instead of above 950 °C. The lower kinetic energy at lower growth temperature can not have adatoms easily move to have good stacking, which leads to more defects and rougher surface. The increase in rms roughness of Mg–GaN with the Mg content, as explained for Fig. 2, is related to the change in the nucleation behavior. The disturbed nucleation can lead to the rougher surface.

Figure 4 shows the carrier concentration, mobility, and electrical conductivity for Mg–GaN films at different Mg contents. The undoped GaN film showed n-type conductivity and had carrier concentration of 1.04×10^{18} cm^{-3}. As the Mg-doping content increased to 5.6 at.% for Mg-0.05 GaN, the carrier concentration decreased to 6.11×10^{16} cm^{-3} and the film remained as an n-type
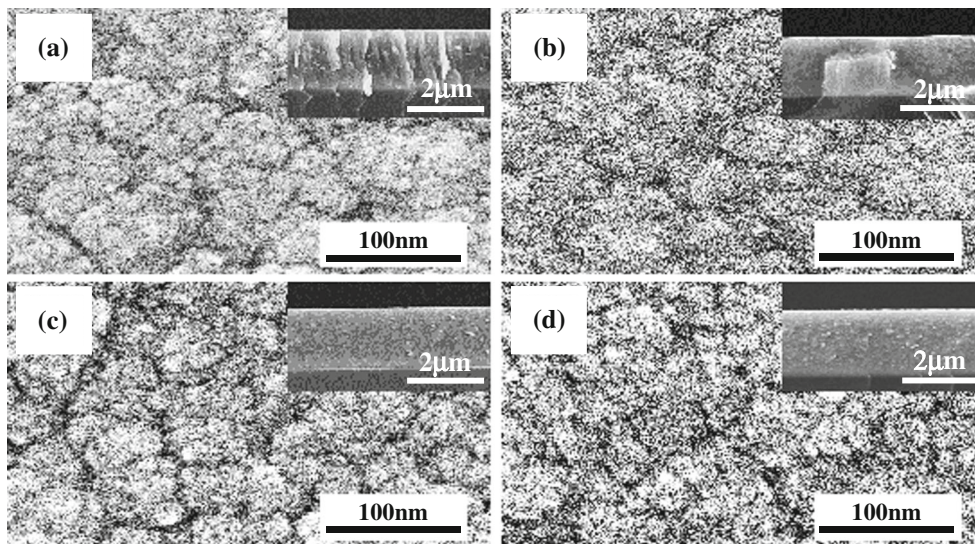
Fig. 2 SEM surface images of Mg-x GaN films at $x =$ **a** 0, **b** 0.05, **c** 0.1, and **d** 0.15. The *insets* are their individual cross-sectional images
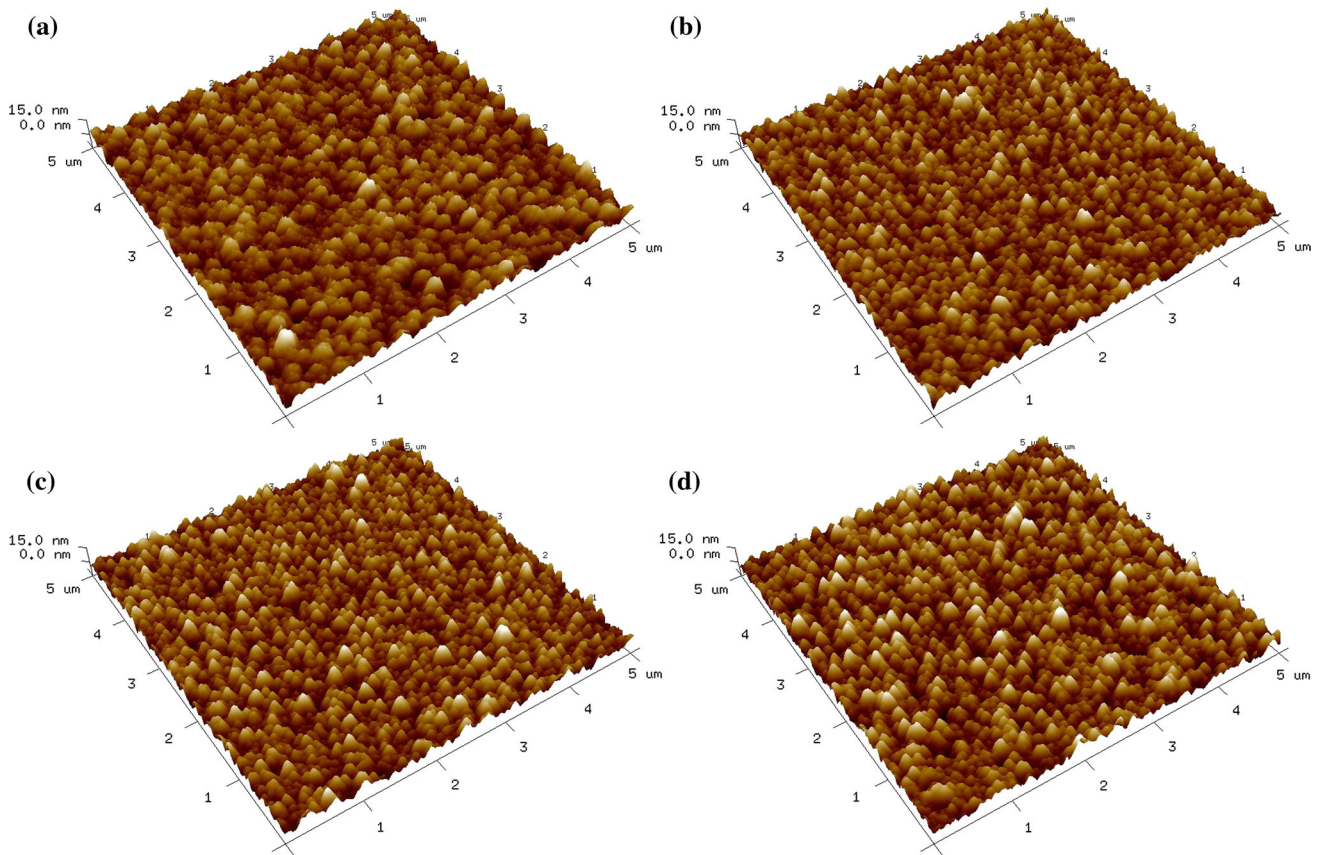

Fig. 3 AFM morphologies of Mg-x GaN films at $x =$ **a** 0, **b** 0.05, **c** 0.1, and **d** 0.15

semiconductor. As the Mg content was 10.2 at%, the Mg-0.1 GaN film transform into p-type conduction and the carrier concentration increased to 9.37×10^{16} cm^{-3}. This value was closed to the previous reports for Mg–GaN

deposited by MOCVD and MBE [6–8]. Here, GaN film with a sufficient Mg content can be directly transformed from n type to p type by reactive sputtering without an annealing procedure. However, when the Mg content
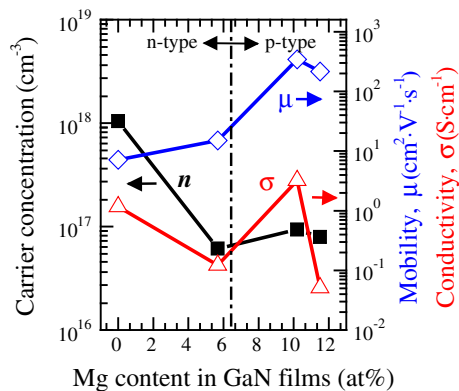
Fig. 4 Electrical properties of carrier concentration, mobility, and electrical conductivity for Mg–GaN films grown at 400 °C with different Mg contents

Fig. 5 Plots of $(\alpha h\upsilon)^2$ versus photon energy $(h\upsilon)$ for the optical band gap determination of Mg–GaN films at different Mg contents

reached 11.5 at.%, the carrier concentration of the Mg-0.15 GaN films slightly dropped to 7.93×10^{16} cm^{-3}. For carrier mobility, they were 7.1, 15.0, 345, and 216 cm^2 V^{-1} s^{-1} for Mg-x GaN with $x = 0$, 0.05, 0.1, and 0.15, respectively. There is a 23-fold increase in mobility as n-type GaN transforms to p-type one. The conductivity related with the carrier concentration and mobility. The Mg-0.1 GaN film had a highest mobility of 345 cm^2 V^{-1} s^{-1} and conductivity of 3.23 S cm^{-1}. The Mg-0.15 GaN film with a high Mg content in target actually can only have 11.5 % Mg incorporated into GaN. It is expected that the over-doping will lead to the dopant precipitation at grain boundary to retard the electrical transport and increase the resistivity. From the above data, the useful Mg content in Mg–GaN films for the p-type conduction exists at a restrictive range. The much refined solubility data for p-type Mg–GaN need further investigations. For MOCVD GaN, thermal annealing is needed to degrade the Mg–H bonding for improved electrical conductivity. However, the sputtering technique without using the metalorganic species and hydrogen atmosphere can avoid the formation of the Mg–H bonding.

To measure the band gap (E_g) of Mg–GaN films, the films were deposited on the transparent glass substrates for measuring absorption spectra at room temperature by UV–vis spectrometer. From the UV–vis measurements, we could calculate the direct energy band gap by using the Tauc Eq. (1) [23].

$$(\alpha h\upsilon)^2 = A(h\upsilon - E_g) \tag{1}$$

where α is absorption coefficient, A is a constant, $h\upsilon$ is the incident photon energy, and E_g is the energy band gap of the test films. The band gap of Mg–GaN films can be obtained by plotting the $(\alpha h\upsilon)^2 - h\upsilon$ curves, followed by extrapolating the linear part of the curves, as shown in Fig. 5. The E_g values were 3.06, 2.99, 2.96 and 2.93 eV for
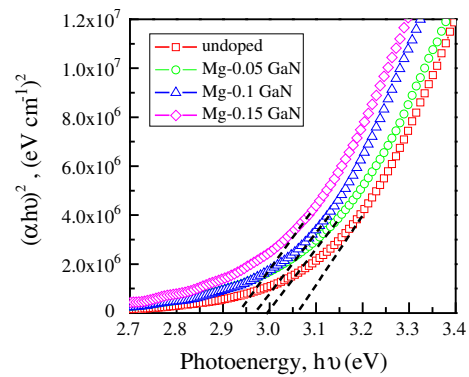
Mg-x GaN at $x = 0$, 0.05, 0.1, and 0.15, respectively. The undoped GaN film showed a smaller band gap than the reported 3.4 eV. However, there were some reports about pure GaN films with an E_g value of $\sim$3.0 eV. Knox-Davies et al. [24] showed Eg of 3.06 eV for their sputtered GaN film measured by the photoluminescence technique and the value increased to 3.64 eV after hydrogenation. GaN films with small E_g can be related to the intrinsic defects. The nitrogen vacancy (V_N) has been proposed as the dominant defect in GaN with a much shallow donor level [25–27]. Ga vacancy in the neutral charge state is a triple acceptor, with a set of levels ranging from 0.2 to 1.1 eV above the valence band edge [28]. That is the donor–acceptor transition in pure GaN to have E_g of $\sim$3.0 eV. For the nitrogen-deficient case or the case with the N/(Mg + Ga) ratio <1, the Ga vacancy is not a thermodynamically stable defect. But under the sputtering condition, the existence of acceptor in n-type GaN is possible due to the disturbance from the sputtering plasma to fail the charge compensation. This can be the reason why the GaN films prepared by sputtering with substrate temperatures at and lower than 400 °C easily show the smaller band gap. For the effect of the Mg content on band gap, the Mg doping in GaN does not have an obvious change in E_g because its acceptor level is +0.2 eV above the valence band maximum [29, 30], close to the acceptor level of Ga vacancy. Therefore, the E_g values of our Mg-doped GaN are related to the donor-to-acceptor transition with the acceptors at two states of Ga vacancy and the Mg-to-Ga (Mg_{Ga}) defects. Li et al. [31] observed that E_g decreased from 3.05 eV for 0.5 % Mg–GaN powder to 2.9 eV for 2.0 % one. Lim et al. [32] observed that the band gap narrowing for high Mg doping concentrations was in the order of 10 meV. In our case, the change in band gap was 60 meV for Mg–GaN with the Mg content increasing from 5.6 to 11.5 %.

To confirm the p-type behavior, a p/n GaN diode is presented. Figure 6 plots the variation of the current–voltage
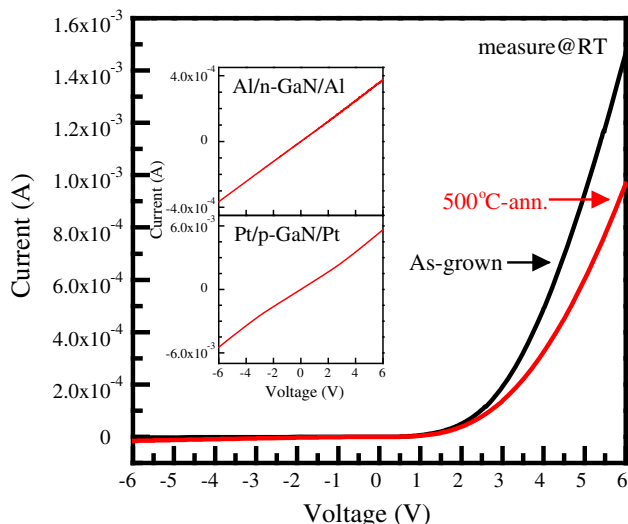
Fig. 6 Typical *I–V* characteristic of as-grown and 500 °C-annealed GaN *p/n* junction diode

(*I–V*) curves of the as-grown and 500 °C-annealed *p/n* GaN diode tested at room temperature. The insets in Fig. 6 showed that Al and Pt electrodes formed ohmic contact with *n*-type and *p*-type GaN films, respectively. The diodes showed a low dark current and had a rectifying behavior. There are no irreversible breakdowns occurred, though the reverse voltage has increased to 20 V. The as-grown and 500 °C-annealed *p/n* GaN diodes with a homojunction had the turn-on voltages of 2.3 and 2.1 V, respectively. The reverse-bias leakage currents at −1 V of the as-grown and 500 °C-annealed diodes were 2.40×10^{-7} A and 1.03×10^{-6} A, respectively.

The ideality factor and barrier height of the as-deposited and annealed *p/n* GaN diodes can be evaluated by the standard diode equation (Eq. 2) based on the thermionic emission theory [33].

$$I = Is \left[\exp\left(\frac{qV}{nkT} \right) - 1 \right] \tag{2}$$

where I_s is the saturation current, q the electron charge, V applied voltage, k the Boltzmann constant $(1.38 \times 10^{-23} \text{ J K}^{-1})$, n the ideality factor, and T the absolute temperature. The saturation current I_s can be expressed as

$$I_s = AA^* T^2 \exp\left(-\frac{q\phi_b}{kT} \right) \tag{3}$$

where A is the device area, A^* the effective Richardson constant equal to 26.4 A cm^{-2} K^{-2} for GaN [34], and ϕ_b the barrier height. With Eq. (3), the barrier height of the *p/n*

GaN diode can be calculated. The ideality factor n is defined as

$$n = \left(\frac{q}{kT} \right) \left(\frac{dV}{d(\ln I)} \right) \tag{4}$$

The ideality factor can be calculated with Eq. (4) by determining the slope of the linear region in a dV-$d(\ln I)$ plot at the forward-bias condition. The ideality factors of the as-grown and 500 °C-annealed diodes were 5.0 and 4.9, respectively. And the barrier heights of the as-grown and annealed diodes were 0.62 and 0.64 eV, respectively. Liu et al. [35] calculated the barrier height of *p/n* GaN junction made by MOCVD was 0.61–0.78. Lee et al. [36] fabricated the similar structure of *p/n* GaN diode by MOVPE. They found that ideality factor of the diode was ∼7. The high ideality factor (n > 2) has been attributed to the high-density structural defects which serve as the trap-assisted generation-recombination centers. The trap-assisted generation-recombination process affects the current transport mechanism of the *p/n* GaN diode.

4 Conclusions

Mg-doped GaN films have been successful deposited on Si (100) substrates by rf reactive sputtering technique at 400 °C with single cermet targets. Mg–GaN films had a wurtzite structure with a preferential nonpolar *m*-(10$\bar{1}$0) crystal plane and excellent adhesion with Si substrates. When the Mg-doping content reached 10.2 at.% in film, the Mg-0.1 GaN film had featureless microstructure and transformed into *p*-type conduction. This *p*-type GaN film had the highest mobility of 345 cm^2 V^{-1} s^{-1} and the highest conductivity of 3.23 S cm^{-1}. The band gap values changed from 3.06 to 2.93 eV as the Mg-doped content in film increased from 0 to 11.5 at.%. All sputtering-made GaN diodes have been demonstrated. The leakage current and ideality factor were 2.40×10^{-7} A and 5.0, respectively, for the as-deposited diode and they were 1.03×10^{-6} A and 4.9 for the annealed one.

References

1. S. Nakamura, T. Mukai, M. Senoh, Jpn J Appl Phys **30**, 1998 (1991)
2. S. Nakamura, M. Senoh, S. Nagahama, N. Iwasa, T. Yamada, T. Matsushita, H. Kiyoku, Y. Sugimoto, Jpn J Appl Phys **35**, 74 (1996)

3. S. Nakamura, Science **281**, 956 (1998)
4. S.C. Jain, M. Willander, J. Narayan, R. Van Overstraeten, J Appl Phys **87**, 965 (2000)
5. H. Amano, M. Kito, K. Hiramatsu, I. Akasaki, Jpn J Appl Phys **28**, 2112 (1989)
6. A. Dussaigne, B. Damilano, J. Brault, J. Massies, E. Feltin, N. Grandjean, J Appl Phys **103**, 013110 (2008)
7. S. Nakamura, T. Mukai, M. Senoh, N. Iwasa, Jpn J Appl Phys **31**, 139 (1992)
8. W.C. Ke, S.R. Jian, I.C. Chen, J.S.-C. Jang, W.K. Chen, J.Y. Juang, Mater Chem Phys **136**, 796 (2012)
9. Y. Chen, H. Wu, G. Yue, Z. Chen, Z. Zheng, Z. Wu, G. Wang, H. Jiang, Appl Phys Express **6**, 041001 (2013)
10. G. Kipshidze, V. Kuryatkov, B. Borisov, Y. Kudryavtsev, R. Asomoza, S. Nikishin, H. Temkin, Appl Phys Lett **80**, 2910 (2002)
11. X. Zhang, S.J. Chua, P. Li, K.B. Chong, W. Wang, Appl Phys Lett **73**, 1772 (1998)
12. Z.X. Zhang, X.J. Pan, T. Wang, E.Q. Xie, L. Jia, J Alloys Compd **467**, 61 (2009)
13. H.W. Kim, N.H. Kim, Appl Surf Sci **236**, 192 (2004)
14. S. Li, M. Ware, J. Wu, P. Minor, Z. Wang, Z. Wu, Y. Jiang, G.J. Salamo, Appl Phys Lett **101**, 122103 (2012)
15. S. Li, T. Zhang, J. Wu, Y. Yang, Z. Wang, Z. Wu, Z. Chen, Y. Jiang, Appl Phys Lett **102**, 062108 (2013)
16. J. Simon, V. Protasenko, C. Lian, H. Xing, D. Jena, Science **327**, 60–64 (2010)
17. J.E. Northrupa, L.T. Romano, J. Neugebauer, Appl Phys Lett **74**, 2319 (1999)
18. R.D. Shannon, C.T. Prewitt, Acta Cryst B **25**, 925 (1969)
19. A.E. Wickenden, D.D. Koleske, R.L. Henry, M.E. Twigg, M. Fatemi, J Cryst Growth **260**, 54 (2004)
20. A. Kikuchi, R. Bannai, K. Kishino, C.M. Lee, J.I. Chyi, Appl Phys Lett **81**, 1729 (2002)
21. S. Strite, H. Morkoç, J Vac Sci Technol, B **10**, 1237 (1992)
22. C.R. Lee, J.Y. Leem, S.K. Noh, S.E. Park, J.I. Lee, C.S. Kim, S.J. Son, K.Y. Leem, J. Crys, Growth **193**, 300 (1998)
23. S. Muthukumaran, R. Gopalakrishnan, Opt Mater **34**, 1946 (2012)
24. E.C. Knox-Davies, S.J. Henley, J.M. Shannon, S.R.P. Silva, J Appl Phys **99**, 036108 (2006)
25. M.G. Ganchenkova, R.M. Nieminen, Phys Rev Lett **96**, 196402 (2006)
26. P. Perlin, T. Suski, H. Teisseyre, M. Leszcznski, I. Grzegory, J. Jun, S. Porowski, P. Bogusławski, J. Bernholc, J.C. Chervin, A. Polian, T.D. Moustakas, Phys Rev Lett **75**, 296 (1995)
27. H.P. Maruska, J.J. Tietjen, Appl Phys Lett **15**, 327 (1969)
28. I. Gorczyca, A. Svane, N.E. Christensen, Solid State Commun **101**, 747 (1997)
29. C. Van de Walle, J. Neugebauer, C. Stampfl, in *Properties, Processing and Applications of GaN Nitride and Related Semiconductors*, ed. by J.H. Edgar, S. Strite, I. Akasaki, H. Amano, C. Wetzel (IEE INSPEC, London, 1999), pp. 275–280
30. J. Orton, C. Foxon, in *Properties, Processing and Applications of GaN Nitride and Related Semiconductors*, ed. by J.H. Edgar, S. Strite, I. Akasaki, H. Amano, C. Wetzel (IEE INSPEC, London, 1999), pp. 300–305
31. H.L. Li, R.J. Xie, N. Hirosaki, B. Dierre, T. Sekiguchi, Y. Yajima, J Am Ceram Soc **91**, 1711 (2008)
32. P.H. Lim, B. Schineller, O. Schön, K. Heime, M. Heuken, J Cryst Growth **205**, 1 (1999)
33. R.K. Gupta, F. Yakuphanoglu, K. Ghosh, P.K. Kahol, Microelectron Eng **88**, 3067 (2011)
34. C.K. Ramesh, V.R. Reddy, C.J. Choi, Mater Sci Eng, B **112**, 30 (2004)
35. Y.J. Liu, D.F. Guo, K.Y. Chu, S.Y. Cheng, J.K. Liou, L.Y. Chen, T.H. Tsai, C.C. Huang, T.Y. Chen, C.S. Hsu, T.Y. Tsai, W.C. Liu, Displays **32**, 330 (2011)
36. M.L. Lee, J.K. Sheu, L.S. Yeh, M.S. Tsai, C.J. Kao, C.J. Tun, S.J. Chang, G.C. Chi, Solid State Electron **46**, 2179 (2002)